2022 30th Mediterranean Conference on Control and Automation (MED)
June 28 - July 1, 2022. Athens, Greece

2022 30th Mediterranean Conference on Control and Automation (MED) | 978-1-6654-0673-4/22/$31.00 ©2022 IEEE | DOI: 10.1109/MED54222.2022.9837222

A Resilient to Faults Auto-Encoder Enabled Kalman based Multi-Sensorial Fusion

Moumita Mukherjee, Avijit Banerjee and George Nikolakopoulos

***Abstract*— This article presents a novel Auto-encoder-enabled fault resilient multi-sensor fusion architecture while incorporating an extended Kalman filter framework. The auto-encoder facilitate reconstruction of the faulty measurements from multiple onboard sensors, while the centralized extended Kalman filter enables an accurate fusion architecture. Moreover, the process is capable of successfully eliminating the additive noise appearing from the raw sensor data. The proposed method provides a robust reconstruction mechanism in the presence of time-dependent anomalies and faulty sensor measurement. The efficacy of the proposed scheme is extensively evaluated in the context of pose estimation for a micro aerial vehicle equipped with multiple onboard sensors. In addition, the evaluation process incorporates various realistic failure scenarios with artificially introduced inaccurate measurements. The superiority of the proposed Auto-encoder enabled centralized Kalman filter (AEKF) fusion is demonstrated through an extensive comparison with a recently developed Fault Resilient Optimal Information Filter (FROIF) method.**

***Index Terms*— Auto-encoder, FROIF, Kalman Filter, Aerial Robot, White Gaussian Noise.**

I. Introduction

A group of sensors may fail to provide accurate information in many areas of field robotics involving an environment that typically presents various difficulties or adversities [1]. For example, in the absence of sufficient illumination conditions, for some part of the surrounding environment, or in the presence of dust particles [2], [3]. Usually, the visual sensors fail to determine the position and orientation of a robotic platform in such a situation, where laser/infrared technology-based sensors could provide additional sensorial information for overcoming this issue [4]. One of the most challenging problems in such a context is the pose estimation of a Micro Aerial Vehicle (MAV) using multiple redundant sensors, where related sensor fusion schemes are utilized to enhance the overall accuracy but also to ensure adequate resiliency at the same time. In general, failure scenarios of the sensor in measurements can be viewed as an abnormal behaviour or deviations from the actual value and could therefore be regarded as outliers.

Generally, signal processing analysis techniques are based on the patterns of sensor measurements concerning time [5]. In this case, signals or sensor measurements can consist of standard signals and a few different types of faults, such as drift faults for a short-term (e.g. 50 to 100 samples), drift faults for a long-term (e.g. more than 1000 samples) or multiple drift faults at separate time intervals with excess noise. In addition, multi sensor fusion approaches based on estimation theory and especially centralized [6] and decentralized fusion [7] approaches using the extended Kalman filter have been used often to get an accurate pose. Though these methods are not sufficient for fault detection and isolation, thus FROIF is introduced as a decentralized fusion framework, incorporating fault detection and isolation framework as it has been presented in [8]. In general, anomaly detection is a challenging task and many approaches have been established in the field of e.g., signal processing [9], [10], state estimation [11], machine learning [12], statistics [13], data mining [14]) for the purpose of outlier detection as well elimination. Therefore, one of the crucial job is to chose one of the method based on the various pattern of faults, faced in real-world applications. The quality of a neural network for classifying information has also been utilized to identify the anomaly in time-series signals. The most popular training method for neural networks is the back-propagation algorithm for feed-forward Neural networks. An Auto-encoder configuration [15] can produce synthetic reconstructed outputs, and it can detect the abnormalities or the deviation in the measurement signal and based on the training of the neural network, it adopts the actual pose patterns of that vehicle, while accordingly is able to repair the faulty part of the signal. As it will be presented in the sequel, those synthetic estimated poses can be useful for the multi-sensor fusion, especially in the cases of sensorial faults.

In light of the presented background, this article aims to establish a novel Auto-encoder-based fusion approach, incorporating the concept of an extended Kalman filter for estimating the pose of a manually operated MAV as the use case under consideration. Thus, the significant contributions of this article are: a) Design of a unique AI-based fusion approach for various ranges of the anomaly to automatically identify the faulty sensor's measurement for each instant, b) Developing synthetic measurement data samples that immensely resemble faultless signals when the raw measurements consist of multiple deviations, c) Employing a multi-input and multi-output extended Kalman filter as a central node to integrate all synthetic poses appearing from the Auto-encoder outcomes, d) Performance evaluation of the proposed Auto-encoder based extended Kalman filter fusion (AEKF) with the help of actual sensor measurements assuming various fault scenarios and comparing the performance with FROIF [8]. The rest of the article continues with a

This work has been partially funded by the European Unions Horizon 2020 Research and Innovation Programme under the Grant Agreement No. 869379 illuMINEation.

The authors are with the Robotics and AI, Department of Computer, Electrical and Space Engineering, Luleå University of Technology, Luleå, Sweden

Corresponding Author's email: moumuk@ltu.se

discussion of the problem formulation in Section II, followed by a comprehensive explanation of the Auto-encoder based Kalman filter (AEKF) framework in Section III. Section IV presents the experimental results demonstrating the method's efficiency, followed by its conclusion in Section V.

II. Problem Formulation

A MAV with a multi-sensorial suit consists of an IMU, a 3D-Velodyne Puck LITE Lidar, a Real-sense camera T265 and an Ultra wide-band. In this case, the acceleration and angular velocity is provided by the IMU and is used as the control inputs. Intel's real-sense camera T265, along with an IMU from Pixhawk 4 flight controller, is used to provide a visual odometry [16], and the 3D-lidar point clouds are also integrated with an IMU for Lidar Inertial Odometry (LIO) [16]. As shown in Fig. 1, the sensors mentioned above are attached in the body-fixed frame $X_B - Y_B - Z_B$ of the MAV. The position of the MAV is described by the conventional East-North-Up (ENU) world frame. Ultimately, the goal is to build a unique and AI-based autonomous estimation incorporating the concept of Auto-encoders to reconstruct the raw measurement signal in the time of fault and a classical extended Kalman filter to calculate the most accurate and noiseless MAV pose. The following nonlinear

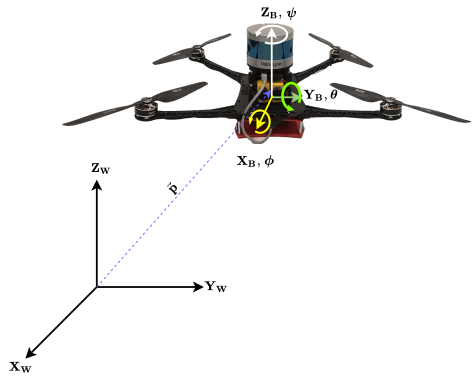

Fig. 1: A schematic representation of the frame of references, the subscript W indicates the global frame and B indicates the body frame

kinematic model for the MAVs is considered as in [17], where the equations of motion are given as:

$$\begin{aligned} \dot{\mathbf{p}} &= \mathbf{v} \\ \dot{\mathbf{v}} &= \mathbf{R}_{\mathbf{B}}^{\mathbf{W}}(\mathbf{q})\left(\mathbf{a}_m - \mathbf{a}_b - \mathbf{a}_n\right) + \mathbf{g} \\ \dot{\mathbf{q}} &= \frac{1}{2}\mathbf{q} \otimes \left(\boldsymbol{\omega}_m - \boldsymbol{\omega}_b - \boldsymbol{\omega}_n\right) \\ \dot{\mathbf{a}}_b &= \mathbf{a}_\omega \\ \dot{\boldsymbol{\omega}}_b &= \boldsymbol{\omega}_\omega \\ \dot{\mathbf{g}} &= \mathbf{0}_{3\times 1} \end{aligned} \tag{1}$$

with $\mathbf{p} \in \mathbb{R}^{3\times1}$ represents the position, $\mathbf{v} \in \mathbb{R}^{3\times1}$ represents the velocity, while $\mathbf{q} \in \mathbb{R}^{4\times1}$ denotes the quaternion for orientation of the MAV. The acceleration and body rates are considered as the input to the kinematic model, a_m and ω_m are measured from an IMU. However, consecutive noisy measurements are stored from the sensors that include a sensor bias as well. $a_b \in \mathbb{R}^{3\times1}$ represents the accelerometer and $\omega_b \in \mathbb{R}^{3\times1}$ represents the gyroscopic bias terms, a_n and ω_n signify the additive noise for the acceleration and the angular rate noise respectively and $g \in \mathbb{R}^{3\times1}$ indicates the gravitational acceleration acting on the MAV. $a_\omega \in \mathbb{R}^{3\times1}$ and $\omega_\omega \in \mathbb{R}^{3\times1}$ are the accelerometer and the gyroscopic process noise respectively. The rotation matrix $R_B^W(q) \in SO(3)$ is introduced to perform the frame transformation from the body to the world frame. The equations of motion for the MAV are expressed in a compact mathematical notation with the following generalized form, provided as:

$$\dot{X} = f(X, u_m, w) \tag{2}$$

$$y_t = [\boldsymbol{I}_{7\times7} \mid \mathbf{0}_{7\times12}]X_t \tag{3}$$

In the experiment, state vector of the MAV is represented as $X = [p, v, q, a_b, \omega_b, g]^T \in R^{19\times1}$, the measured input with noise is based on IMU reading and indicated as $u_m \in R^{6\times1}$ and $w \in R^{6\times1}$ represents the random process noise.

III. Methodology

In this article, an Auto-encoder based Extended Kalman filter is demonstrated. A framework of three main layers and a few sub-layers provides a more accurate and noiseless pose than the other fusion methods often used for the multi-sensor fusion, especially when the measurement signals contain multiple faults and excess noise. Essentially, there are three layers as depicted in Fig 2: the first module or sensor module that provides raw measurement data (position and orientation information of the MAV), secondly, the auto-encoders and the last layer consist of the extended Kalman filter that fuses all the reconstructed outputs in a single node appearing from the second layer (Auto-encoders). This article employs

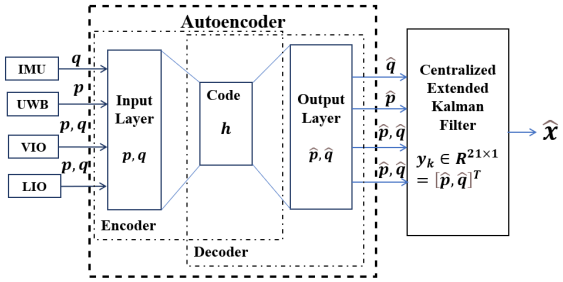

Fig. 2: Schematic representation of Auto-encoder enabled Extended Kalman Filter

the supervised auto-encoder to reconstruct the faulty signal where a Vicon motion capture system provides the ground truth. Thus, the Vicon motion camera pose is used to train the auto-encoders, as illustrated in the Figure 3. Once the neural network of the auto-encoders has adopted the actual signal pattern's behaviour, it will eventually be able to generate more accurate position and orientation signals. Each Auto-encoder consist of three separate neural network layers that are the encoders, coders, and decoders. The primary

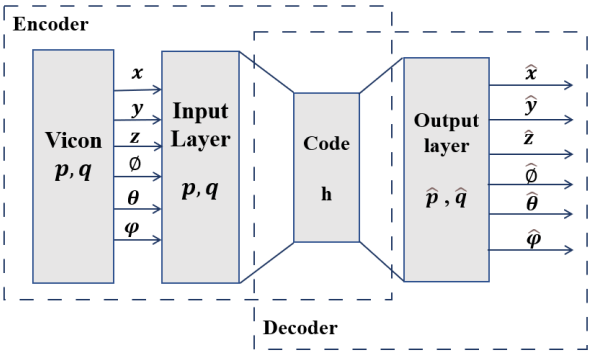

Fig. 3: Illustrative training mechanism for a three-layer auto-encoder structure

objective is to reduce the order of the input data samples by extracting features with low dimensions. The Auto-encoder's input signal can undergo a compression in codes with lower dimensions when it passes through the encoder section. An encoder transforms the input into the more abstract feature vectors, and a decoder reconstructs the information from the feature vectors and yields the synthetic data samples. Fig. 2 represents the fundamental auto-encoder configuration that is embedded with the extended Kalman filter and output synthetic data samples are fed back to the Kalman filter module for the correction steps. Each auto-encoder is utilized in Eq. 4 and Eq. 5 to reconstruct the input signal(x). In Eq. 4 the input(x) is multiplied by the optimal weight $z^{(1)}$ by using a back-propagation learning algorithm and added with the bias $b^{(1)}$. These two terms provide the function $h^{(1)}$ and the output variable $z^{(1)}$ is sent to the second layer of the activation function, which is denoted as $h^{(2)}$ in Eq. 5. Hence, The reconstructed estimated signal $\hat{x}$ is produced with the help of the second layer of the activation function $h^{(2)}$.

$$z^{(1)} = h^{(1)}(w^{(1)}x + b^{(1)}) \tag{4}$$

$$\hat{x} = h^{(2)}(w^{(2)}z^{(1)} + b^{(2)}) \tag{5}$$

Centralized Extended Kalman filter: In discrete-time nonlinear dynamical systems, the Extended Kalman Filter effectively calculates the approximate maximum-likelihood estimates and eventually, the EKF is employed with a multi-dimensional input and output framework to remove noise from the Auto-encoders' reconstructed poses and combine all positions and orientations in a single node. Fig. 2 depicts the input and output signals of the Auto-encoder based extended Kalman filter. The equations of motion for the manually flown MAVs are represented mathematically by Equ. 6a and Equ. 6b

System Dynamics:

$$x_k = f_{k-1}(x_{k-1}, u_{k-1}, \omega_{k-1}) \tag{6a}$$

$$y_k = h_k(x_k, v_k) = [\boldsymbol{I}_{7\times 7} \mid \mathbf{0}_{7\times 12}]x_k + v_k \tag{6b}$$

Whereas k represents the discrete-time instants and the model inaccuracy is addressed by considering a process noise $\omega_k \in \mathbf{R}^{19}$. Additionally, a measurement noise vector $v_k \in \mathbf{R}^7$ is introduced in Eq. (6b) to describe a realistic output model, under the influence of noisy measurements from embedded sensors. The process and measurement noise are assumed to follow the Gaussian distribution as:

$$\omega_k \sim \mathcal{N}(0,\, Q_k), v_k \sim \mathcal{N}(0,\, R_k) \tag{7}$$

where Q_k and R_k denotes the process noise co-variance matrix and the measurement noise co-variance matrix, respectively. The mathematical operator E denotes the expectation and the superscript T indicates the transpose. Initiating with an primary prediction of a posteriori estimate $\hat{x}_0^+ = E(x_0)$ and $P_0^+ = E[(x-\hat{x}_0^+)(x-\hat{x}_0^+)^T]$, along with the assumption in Equation (7), the central node of EKF is described as the following prediction-correction formalism:

Prediction Steps:

$$\hat{x}_0^+ = E(x_0), P_0^+ = E[(x-\hat{x}_0^+)(x-\hat{x}_0^+)^T] \tag{8a}$$

$$\hat{x}_k^- = f_{k-1}(\hat{x}_{k-1}^+, u_{k-1}, 0) \tag{8b}$$

$$K_k = P_k^- H_k^T (H_k P_k^- H_k^T + R_k^T)^{-1} \tag{8c}$$

$$P_k^- = F_k P_k^+ F_k^T + L_k Q_k L_k \tag{8d}$$

where the '$+$' symbol is used to denote an a priori estimate, the '$-$' symbol is designated to a posteriori estimate, The Jacobian matrices are defined as:

$$F_k = \frac{\partial f_{k-1}}{\partial x_k},\ L_k = \frac{\partial f_k}{\partial u_k},\ H_k = \frac{\partial h_k}{\partial x_k} \tag{9}$$

while the inputs excitation u_k (linear acceleration and angular velocity), used in the prediction process, are essentially obtained from the IMU measurements.

Correction Steps:

$$\hat{x}_k^+ = \hat{x}_k^- + K_k[y_{c_k} - h_k(x_k^-, 0)] \tag{10a}$$

$$P_k^+ = (I - K_k H_k)P_k^- \tag{10b}$$

where, the measurement vector (y_{c_k}) is described as:

$$y_{c_k} \in \mathbb{R}^{21\times 1} = [\hat{p}_{LIO}, \hat{q}_{LIO}, \hat{p}_{VIO}, \hat{q}_{VIO}, \hat{p}_{UWB}, \hat{q}_{IMU}]^T \tag{11}$$

Since the EKF central node removes the noise from the Auto-encoder measurements, the reconstructed measurements ($\hat{p}, \hat{q}$) from the multiple sensors are taken into account collectively as a multi-output (y_{c_k}) in the Eq. 11, In addition, the measurement noise co-variance matrix R_k, Kalman gain K_k, and output gradient H_k are reconsidered.

IV. Simulation Results

A manually operated MAV equipped with multiple pose sensors onboard is flown through an approximate rectangular trajectory. The measurement data collected from various onboard sensors are used to evaluate the uniquely proposed localization framework considering the Auto-encoder-based Kalman filter scheme. In order to demonstrate the resiliency of the proposed AEKF pose estimation approach, simulated pseudo faults are considered to be artificially introduced in different sensor measurement data over multiple time instants. In this experiment, the absences of the proper illumination and presence of dust particle in the environment

creats faults in measurements coming from the sensor like Real-sense camera whereas Lidar and UWB can provide the faultless measurement signals. The accuracy of the estimated pose obtained from AEKF are compared with the outcomes from a highly accurate VICON motion capture system, comprised of 19 cameras, which yields a precision in the sub-millimetre range, serving as the ground truth. Moreover, a comparison of the proposed AEKF method with the recently developed fault-tolerant multi-sensor fusion approach FROIF [8] is presented. Unlike FROIF, which explicitly embeds an analytical optimization framework for fault detection and isolation features, the proposed AEKF emphasizes neural-network-based autoencoders that have the capability to reconstruct the signal so that the signal with fault is regenerated to fix the error. Eventually, it provides such signals that effectively eliminates underlying fault and measurement noise. As a result, the fusion with such regenerated signals essentially provides a pose estimation free from faulty measurements. Four different realistic situations are considered in the present analysis to extensively demonstrate the resiliency of the AEKF in the presence of faulty measurement as follows:

- **Case-1: Without faults** No artificially created fault is introduced in the sensor measurements.
- **Case-2: Temporal faults for shorter period of time in single sensor** A pseudo-temporal failure is introduced between $(20-20.2)s$ and $(45-45.2)s$ in the Visual Odometry (VIO) while all other measurements are unaffected.
- **Case-3: Multiple temporal fault with shorter and longer period of time in multiple sensor measurements** Pseudo temporary erroneous measures are introduced between $(20-20.2)s, (25-25.5)s$, and $(30-30.5)s$ in Visual Odometry(VIO). In addition, UWB is corrupted during $(40-40.5)s$ and $(50-50.2)s$. In contrast, the measurements from all other sensors remain unchanged.
- **Case-4: Multiple temporal failure in Multiple sensor with excess noise** Pseudo temporary erroneous measures are introduced between $(20-20.2)s, (25-25.5)s$, and $(30-30.5)s$ with additional white Gaussian noise. In addition, UWB is corrupted during $(40-40.5)$ s and $(50-50.2)s$. In contrast, the measurements from all other sensors remain unchanged

Thus, the poses appearing from the Vicon camera are used once to train the neural networks involved in the auto encoder. Fig 3 depicts the schematics of data flow during the training process of an Auto-encoder. However when the auto encoders cope up with the pattern of the measurement signals, it has been used for generating the synthetic data samples from raw measurement signals. Afterward, those synthetic data samples are collectively fused in single node using the extended Kalman filter, as mentioned in section III.

In the centralized EKF, the process and measurement noise covariances are considered as $Q_k = 10\times\ I_{19\times19}$, $R_k = 1000 \times I_{21\times21}$ respectively. The initial state $X_0 = [0_{1\times6}, 1, 0_{1\times11}, 9.81]^T$ and initial error co-variance is considered as $P_0 = I_{19\times19}$. The pose of the MAV is estimated using AEKF and a comparison with FROIF [8] is presented along with the ground truth trajectory obtained from Vicon camera. All raw data measurement samples in Case-1 are considered almost accurate and faultless, and the estimated trajectory is shown in Fig. 4. In addition, estimated transnational position and orientation of the MAV are the component wise presented in Fig 5 and Fig 6 respectively. It can be observed from the Figs. 5 6 that the pose estimation from AEKF and FROIF are fairly comparable when we considered no faults in the real sensor measurements. Figs 7 and 8 presented semi logarithmic Root Mean Square Error (RMSLE) between the pose observed from the Vicon motion capture system and the associated estimated pose using the proposed AEKF. Figure 9 represents the performance of AEKF and FROIF associated with the conditions for Case 2, which deals with

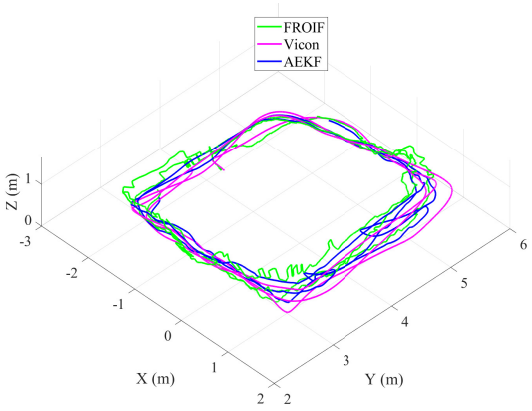

Fig. 4: Case-1: Variation of estimated trajectory obtained from AEKF, FROIF and Vicon based ground truth

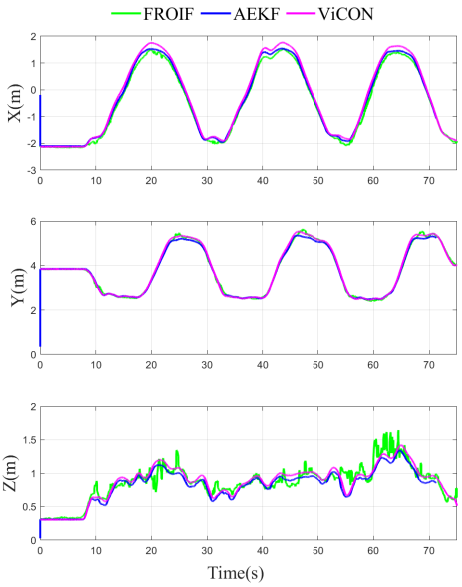

Fig. 5: Case-1: Time history of estimated MAV positions using AEKF and FROIF

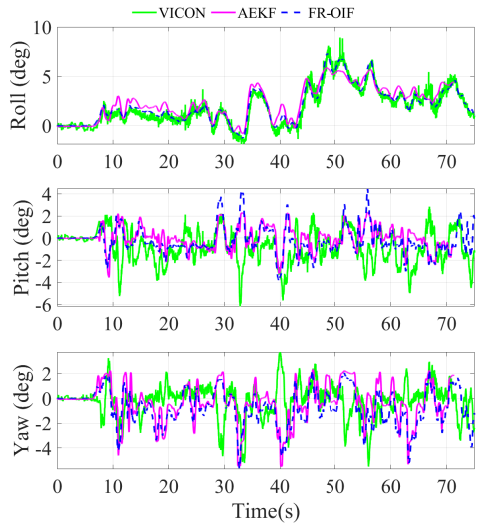

Fig. 6: Case-1: Variation of estimated orientation of MAV in Euler angles using AEKF and FROIF

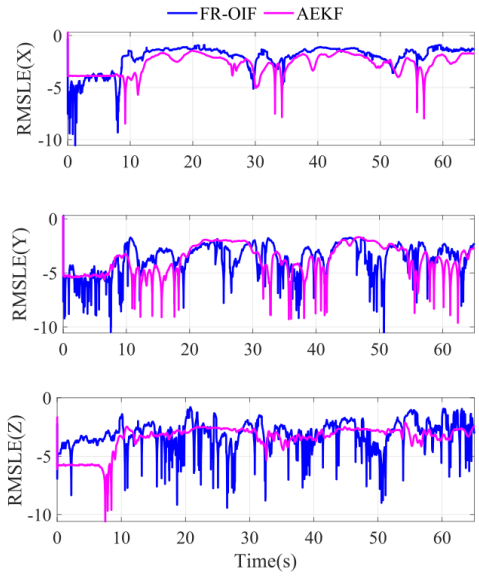

Fig. 7: Case-1: Root Mean Square Error in semi-logarithmic scale for estimated positions

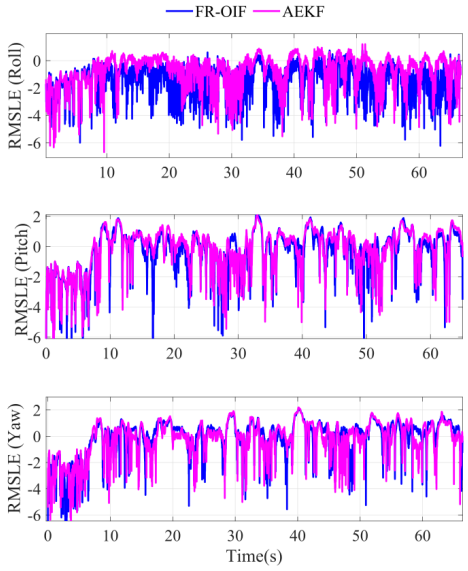

Fig. 8: Case-1: Root Mean Square Error in semi-logarithmic scale for the estimated orientation

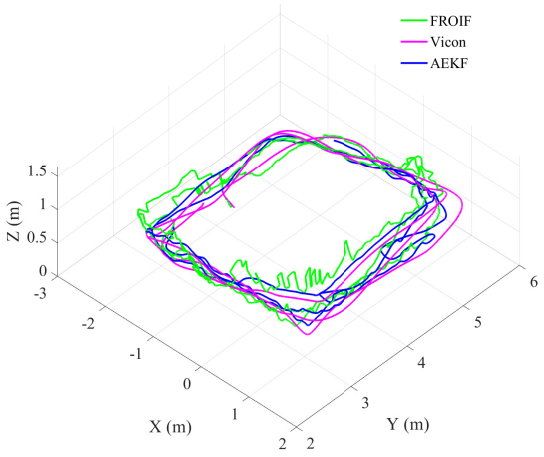

Fig. 9: Case 2: Variation of estimated trajectory obtained from AEKF, FROIF and ground truth, in presence of temporary failure in VIO measurements

multiple faults appeared in the raw data measurement in different operation period. However, the condition depicted here considers the presence of faults in visual odometry only, which is appearing at different operating times at $(20-20.2)s$ and $(45-45.2)s$ respectively. Estimated pose obtained based on AEKF and FROIF for the above mentioned scenario is presented in Fig 10. In the sequel the performance is compared with the ground truth poses, thus Fig 11 and 12 depict the RMSE performance in semi-logarithmic scale. It can be observed that the performance of proposed AEKF is comparatively superior when fault occurs in visual odometry measurements. Apart from the above mentioned scenario the present analysis have considered two more distinct cases. In Case-3, multiple sensor failures (for the present study both VIO and UWB) are introduced in different operating points. Figure 13 represent the performance of AEKF and FROIF for the multiple sensor failure scenarios. Correspondingly, the variation of RMSLE are presented in Figs. (15-18). One can observe that the estimation errors obtained from AEKF are more negative compared to the FROIF based estimation. According to RMSLE analysis, the more negative error in the logarithmic scale represents relatively accurate estimation. Eventually, it is evident from the performance(15-18) of the proposed AEKF that it can provide a resilient and precise pose estimation which is very close to the ground truth under a variety of sensor failure scenarios. A more realistic condition with highly noisy measurement data along with multiple sensor failure is considered for the Case 4. Addi-

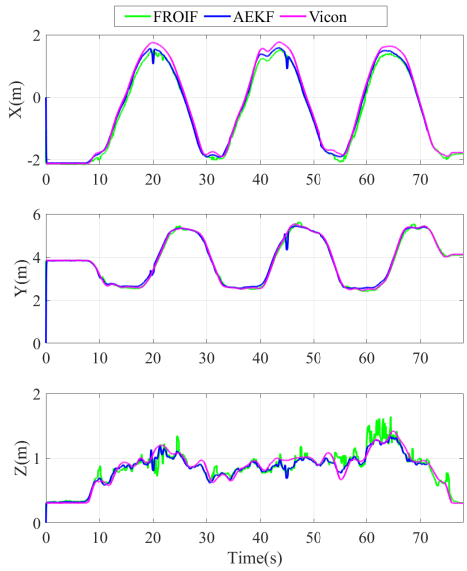

Fig. 10: Case-2: Time history of estimated MAV positions using AEKF and FROIF

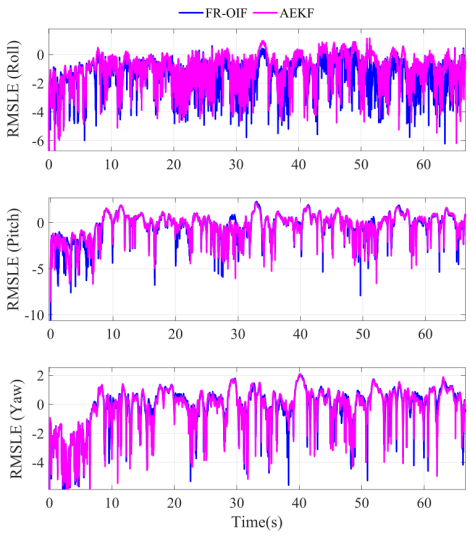

Fig. 12: Case 2: Logarithmic Root Mean Square Error in estimated orientation, in presence of temporary failure in VIO

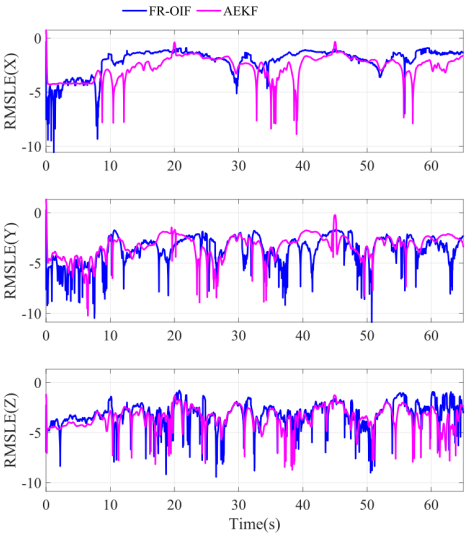

Fig. 11: Case 2: Logarithmic Root Mean Square Error in estimated position, in presence of temporary failure in VIO

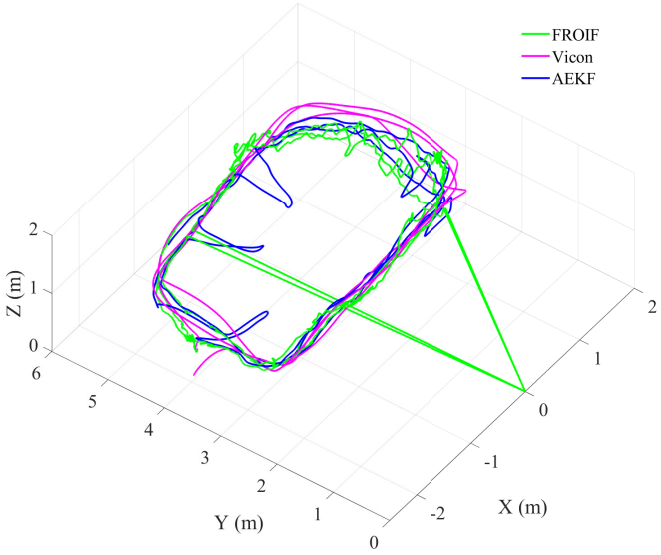

Fig. 13: Case-3: Estimated trajectory with temporal failure in VIO and UWB at different operating points

tional Gaussian noise with zero mean and $v_k \sim \mathcal{N}(0, 0.1)$ variance is injected artificially into the measurement data to demonstrate the effectiveness of AEKF in the presence of high noisy environment. Moreover, it can be concluded from the simulation results that the AEKF is more resilient than the FROIF when multiple faults occur in different sensor measurements along with presence of excess noise.

V. Conclusion

In this article, an Auto-encoder based fusion framework (AEKF) is presented with simulation results. The proposed framework with three principal layers and a few sub-layers achieves a more accurate and noiseless pose than with the other fusion method often used for the multi-sensor fusion, especially when the measurement signals are subject to multiple faults. However, few failure scenarios in measurement signals are artificially integrated to prove the effectiveness of the proposed method. Significantly, the performance of AEKF is compared with FROIF for checking the resiliency during situations when the fault occurs in multiple operating times in a single sensor or multiple sensors corrupted from heavy noise. Multiple pose information, appearing from the Auto-encoder, are integrated at a single node using the EKF to create more accurate and noiseless estimated poses for the MAV. All the outcomes are integrated using the EKF, and thus the proposed framework could be called a centralized

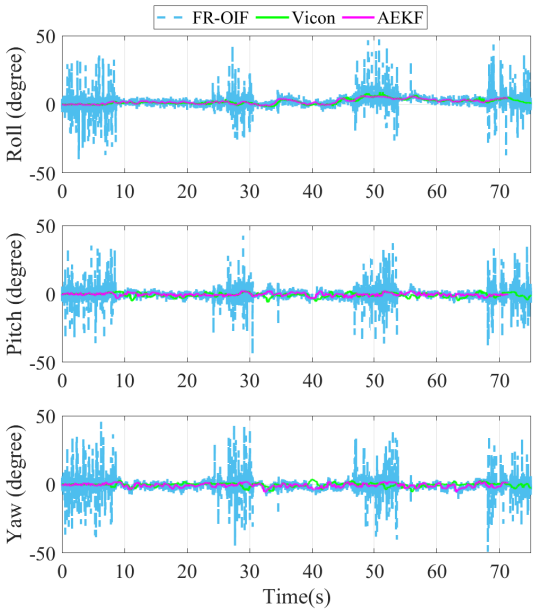

Fig. 14: Case 4: Estimated orientation with temporal failures VIO and UWB measurements and additive noise

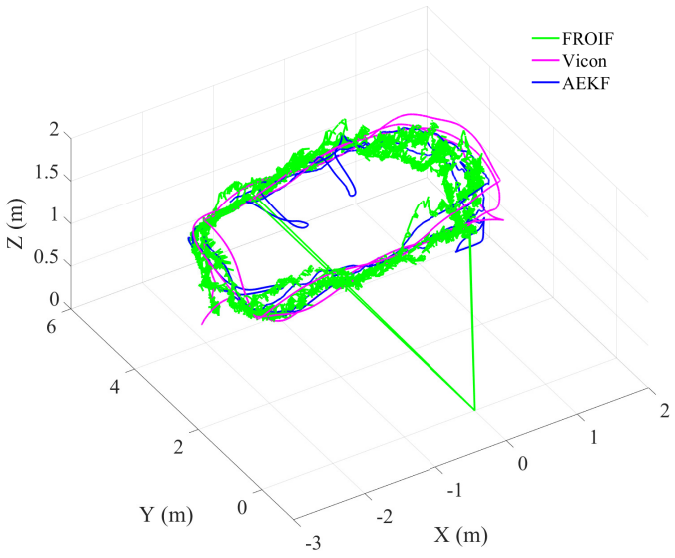

Fig. 15: Case 4: Variation of estimated trajectory with temporal failure in VIO and UWB and additive noise

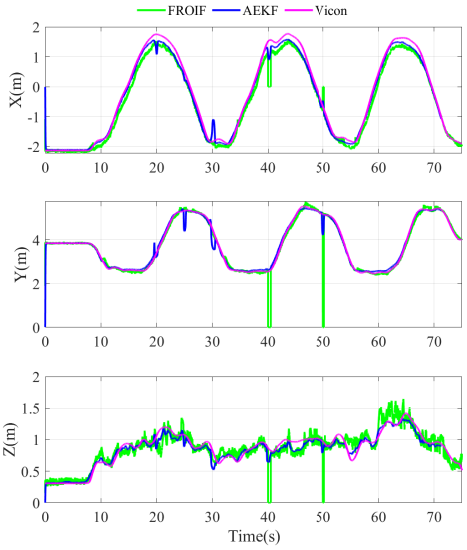

Fig. 16: Case 4: Time history of estimated position using AEKF and FROIF

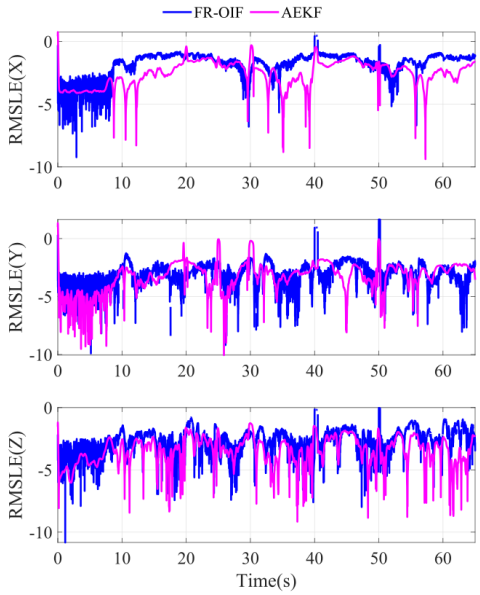

Fig. 17: Case 4: Root Mean Square Error in semi-logarithmic scale in estimated position

Kalman filter based fusion approach. Various possible faults that can be occurred during the measurements are considered in this article to evaluate the method's effectiveness. Hence, from the comparative results, the proposed Auto-encoder-based centralized Kalman filter fusion approach (AEKF) outperforms the Fault resilient optimal information filter (FROIF) for various anomaly ranges with excess noise.

REFERENCES

[1] A. Agha, K. Otsu, B. Morrell, D. D. Fan, R. Thakker, A. Santamaria-Navarro, S.-K. Kim, A. Bouman, X. Lei, J. Edlund *et al.*, "Nebula: Quest for robotic autonomy in challenging environments; team costar at the darpa subterranean challenge," *arXiv preprint arXiv:2103.11470*, 2021.

[2] S. S. Mansouri, C. Kanellakis, D. Kominiak, and G. Nikolakopoulos, "Deploying mavs for autonomous navigation in dark underground mine environments," *Robotics and Autonomous Systems*, vol. 126, p. 103472, 2020.

[3] C. Kanellakis, S. S. Mansouri, G. Georgoulas, and G. Nikolakopoulos, "Towards autonomous surveying of underground mine using mavs," in *International Conference on Robotics in Alpe-Adria Danube Region*. Springer, 2018, pp. 173–180.

[4] P. Fritsche, S. Kueppers, G. Briese, and B. Wagner, "Radar and lidar sensorfusion in low visibility environments." in *ICINCO (2)*, 2016, pp. 30–36.

[5] M. O. Mustafa, D. Varagnolo, G. Nikolakopoulos, and T. Gustafsson,

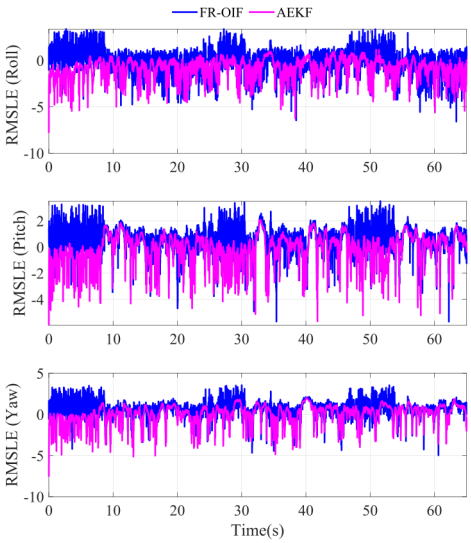

Fig. 18: Case 4: Logarithmic Root Mean Square Error in estimated orientation

"Detecting broken rotor bars in induction motors with model-based support vector classifiers," *Control Engineering Practice*, vol. 52, pp. 15–23, 2016.

[6] N. Sahu, R. Gupta, A. Kumar, R. Bahl, and I. N. Kar, "Centralized kalman filter for fusion of multiple on-board auxiliary sensors with ins for underwater navigation," in *2019 IEEE Underwater Technology (UT)*, 2019, pp. 1–6.

[7] S.-L. Sun and Z.-L. Deng, "Multi-sensor optimal information fusion kalman filter," *Automatica*, vol. 40, no. 6, pp. 1017–1023, 2004.

[8] M. Mukherjee, A. Banerjee, A. Papadimitriou, S. S. Mansouri, and G. Nikolakopoulos, "A decentralized sensor fusion scheme for multi sensorial fault resilient pose estimation," *Sensors*, vol. 21, no. 24, 2021.

[9] W. Lu and A. A. Ghorbani, "Network anomaly detection based on wavelet analysis," *EURASIP Journal on Advances in Signal Processing*, vol. 2009, pp. 1–16, 2008.

[10] Z. Chen and W. Li, "Multisensor feature fusion for bearing fault diagnosis using sparse autoencoder and deep belief network," *IEEE Transactions on Instrumentation and Measurement*, vol. 66, no. 7, pp. 1693–1702, 2017.

[11] A. Ashok, M. Govindarasu, and V. Ajjarapu, "Model-based anomaly detection for power system state estimation," *Advances in Electric Power and Energy: Static State Estimation*, pp. 99–121, 2020.

[12] P. K. Chan, M. V. Mahoney, and M. H. Arshad, "A machine learning approach to anomaly detection," Tech. Rep., 2003.

[13] P. J. Rousseeuw and M. Hubert, "Anomaly detection by robust statistics," *Wiley Interdisciplinary Reviews: Data Mining and Knowledge Discovery*, vol. 8, no. 2, p. e1236, 2018.

[14] S. Agrawal and J. Agrawal, "Survey on anomaly detection using data mining techniques," *Procedia Computer Science*, vol. 60, pp. 708–713, 2015.

[15] T. H. Dwiputranto, N. A. Setiawan, and T. B. Aji, "Machinery equipment early fault detection using artificial neural network based autoencoder," in *2017 3rd International Conference on Science and Technology-Computer (ICST)*. IEEE, 2017, pp. 66–69.

[16] T. Shan, B. Englot, D. Meyers, W. Wang, C. Ratti, and R. Daniela, "Lio-sam: Tightly-coupled lidar inertial odometry via smoothing and mapping," in *IEEE/RSJ International Conference on Intelligent Robots and Systems (IROS)*. IEEE, 2020, pp. 5135–5142.

[17] A. Santamaria-Navarro, G. Loianno, J. Sola, V. Kumar, and J. Andrade-Cetto, "Autonomous navigation of micro aerial vehicles using high-rate and low-cost sensors," *Autonomous robots*, vol. 42, no. 6, pp. 1263–1280, 2018.